ELSEVIER

Materials Science and Engineering A 486 (2008) 215–221

MATERIALS SCIENCE & ENGINEERING A

www.elsevier.com/locate/msea

Microstructures, densification and mechanical properties of $TiC–Al_2O_3–Al$ composite by field-activated combustion synthesis

Qiaodan Hu [a], Peng Luo [b], Youwei Yan [a,*]

[a] *State Key Laboratory of Materials Processing and Die & Mould Technology, Huazhong University of Science & Technology, Wuhan 430074, China*

[b] *National Engineering Research Center of Light Alloys Net Forming, Shanghai Jiao Tong University, Shanghai 200240, China*

Received 21 July 2007; received in revised form 29 August 2007; accepted 30 August 2007

Abstract

Dense $TiC–Al_2O_3–Al$ composite was prepared with Al, C and TiO_2 powders by means of electric field-activated combustion synthesis and infiltration of the molten metal (here Al) into the synthesized $TiC–Al_2O_3$ ceramic. An external electric field can effectively improve the adiabatic combustion temperature of the reactive system and overcome the thermodynamic limitation of reaction with $x < 10$ mol. Thereby, it can induce a self-sustaining combustion synthesis process. During the formation of $Al_2O_3–TiC–Al$ composite, Al is molten first, and reacted with TiO_2 to form Al_2O_3, followed by the formation of TiC through the reaction between the displaced Ti and C. Highly dense $TiC–Al_2O_3–Al$ with relative density of up to 92.5% was directly fabricated with the application of a 14 mol excess Al content and a 25 V cm^{-1} field strength, in which TiC and Al_2O_3 particles possess fine-structured sizes of 0.2–1.0 μm, with uniform distribution in metal Al. The hardness, bending strength and fracture toughness of the synthesized $TiC–Al_2O_3–Al$ composite are 56.5 GPa, 531 MPa and 10.96 MPa m$^{1/2}$, respectively.

Keywords: Field-activated combustion synthesis (FACS); $TiC–Al_2O_3–Al$ composite; Microstructures; Densification; Mechanical properties

1. Introduction

The high specific strength and stiffness, good toughness and wear resistance of $TiC–Al_2O_3–Al$ composite have attracted considerable attention in fields of aeronautics, astronautics, automobile industries [1,2], etc. Up to date, combustion synthesis (CS) or self-propagating high-temperature synthesis (SHS) [3–5] has been one of the most important techniques for fabrication of cermet composites. Meanwhile, bottleneck of densification limits its porous products for practical structural applications [6,7]. Thus, integration of SHS with densification means has been an important development direction. Various densification techniques have been developed, including SHS-QP (quick press) [8], SHS-QHIP (quasi-hot-isostatic-press) [9], SHS-Forging [10], etc., most of which can produce a fully dense samples, but also incur an economic penalty simultaneously.

Feng et al. [1] proposed a process to enhance the densification, by allowing the liquid metal generated during combustion synthesis to simultaneously infiltrate into the synthesized porous ceramic matrix. Compared with SHS-QP, SHS-QHIP and SHS-Forging, as mentioned above, this method retains the advantages of SHS process and can be free of further densification means.

For $3TiO_2–3C–(4+x)Al$ system, the results obtained by Feng et al. [1] testify that if the excess Al content, x, is more than 9 mol, it will be impossible to initiate reaction of the system because its adiabatic combustion temperature is below 1800 K, the empirically established minimum temperature for the thermodynamic limitation of SHS reactions [11]. Thus, in the work by Feng et al., merely CS system with $x \leq 9$ mol can be initiated, and the relative density of the synthesized composites is practically lower than 80% of its theoretical prediction.

At the same time, there exists a technological contradiction in CS of $TiC–Al_2O_3–Al$ composite. On the one hand, more excess amount of molten Al infiltrate into $TiC–Al_2O_3$, favoring the enhancement of densification. On the other hand, due to more decalescence, the adiabatic temperature will decrease below the

* Corresponding author. Tel.: +86 27 87543876; fax: +86 27 87541922.
E-mail address: yanyw@mail.hust.edu.cn (Y. Yan).

0921-5093/$ – see front matter © 2007 Elsevier B.V. All rights reserved.
doi:10.1016/j.msea.2007.08.075

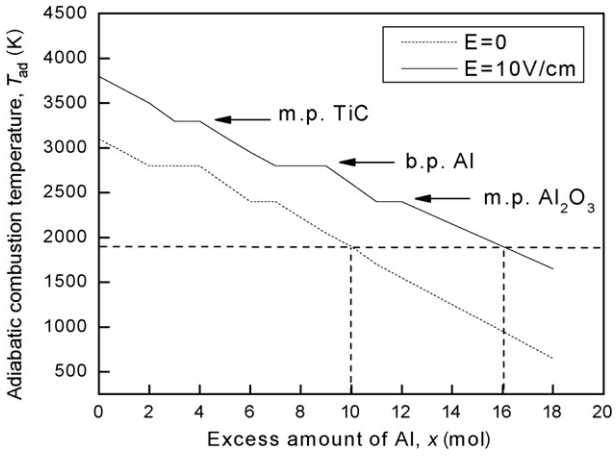

Fig. 1. The dependence of adiabatic combustion temperature on excess Al content at different electric field strength in the synthesis of TiC–Al_2O_3–Al.

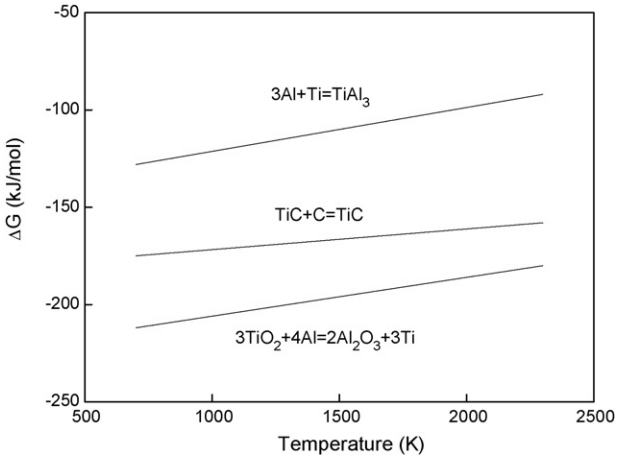

Fig. 3. Gibbs energy of Al_2O_3, TiC and $AlTi_3$ at different temperature.

threshold value (1800 K) and the SHS reaction cannot take place or self-sustain.

Recently, a new method, referred as field-activated combustion synthesis (FACS) [12], based on the use of an external electric field to activate self-propagating reactions of some systems with low reaction enthalpy or a relatively low adiabatic temperature, has been developed and used to synthesize a lot of materials difficult to be synthesized with common SHS process, those include SiC–AlN, B_4C–TiB_2, Ti_3Al [13–16], etc.

In this work, we apply FACS with the infiltration of molten Al generated during the process into the synthesized products to prepare dense TiC–Al_2O_3–Al composite directly, whose combustion thermodynamics, microstructures, densification and mechanical properties were investigated in detail.

2. Experimental

The TiC–Al_2O_3–Al composite from starting powders of Al, C and TiO_2 was prepared by the reaction as

$$3TiO_2 + 3C + (4+x)Al = 3TiC + 2Al_2O_3 + xAl \quad (1)$$

Powders of 99% TiO_2, 99% Al and 99.7% C were used as starting materials with a sieve classification of −300, −200 and −350 mesh, respectively. The powders were dry-mixed in a mechanical shaker for about 24 h, in the desired stoichiometry (Eq. (1)) with excess Al content x from 0 to 14 mol. Correspondingly, theoretical volume percentages of TiC and Al_2O_3 in the final products are over the range 41.5–15.9% and 58.5–22.6%, respectively. Green compacts were produced by cold-pressing the powder mixtures to form samples with dimensions of 25 mm × 20 mm × 20 mm and the relative green density with 50%. The specimens were placed between a pair of spring-loaded graphite electrodes. Ignition was accomplished by a tungsten heating coil placed near one end of the sample while a voltage was applied across the graphite electrodes. The SHS experiments were carried out inside a steel pressure chamber under an argon atmosphere by applying a pressure of about 0.1 MPa.

The combustion temperature was measured by a two-color optical pyrometer (Incon Modline R) with a response time of 10 ms. The propagation velocity of combustion wave was

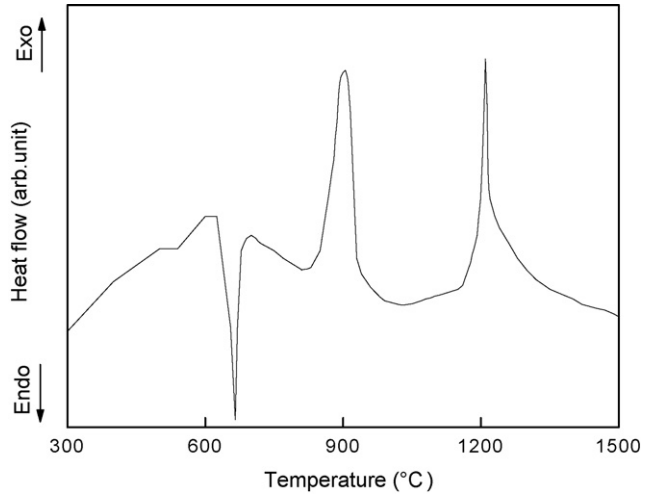

Fig. 2. DTA curve of TiO_2–C–Al system.

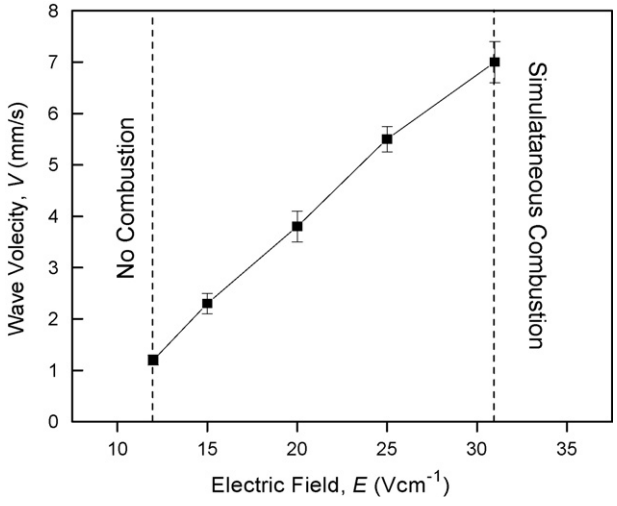

Fig. 4. The effect of electric field strength on the propagation wave velocity in the synthesis of TiC–Al_2O_3–Al.

determined by timing of the propagation from one end of the sample to the other. The porosity and density of the combustion products were measured by Archimedes method. The product was electrical-discharge machined to specimens and then ground and polished. The combustion products were identified by X-ray diffraction analysis and their microstructures were determined from scanning electron microscopy (SEM) with energy dispersive (EDS) analysis. The fracture toughness was tested by single-edge notched bend (SENB) method, under the cross-head speed 0.5 mm/min. The size of the specimen was 2 mm × 4 mm × 20 mm, with notch width 0.2 mm and depth 1.6 mm. The bending strength was tested by the three-point bending method using a testing machine (MTS SINTECH). The size of specimens was 3 mm × 4 mm × 20 mm and the hardness was tested using HR-150A tester. An average of five measurements was adopted to represent the mechanical properties.

3. Results and discussions

3.1. Thermodynamics and DTA analysis

Calculations of the adiabatic combustion temperature (T_{ad}) of the TiO_2–C–Al reaction as functions of the excess Al content, x, and the field strength, E, are presented in Fig. 1. Details of the calculations have been discussed by Hu et al. [17]. The figure shows that the T_{ad} decreased with the increasing Al residual amount, x, with or without the electric field. In absence of field, the adiabatic combustion temperature decreased under the threshold value (1800 K) with $x \geq 10$ mol, which made the reaction not be self-sustain. However, in presence of field, the adiabatic temperature increased due to the Joule heating. Thus, the imposition

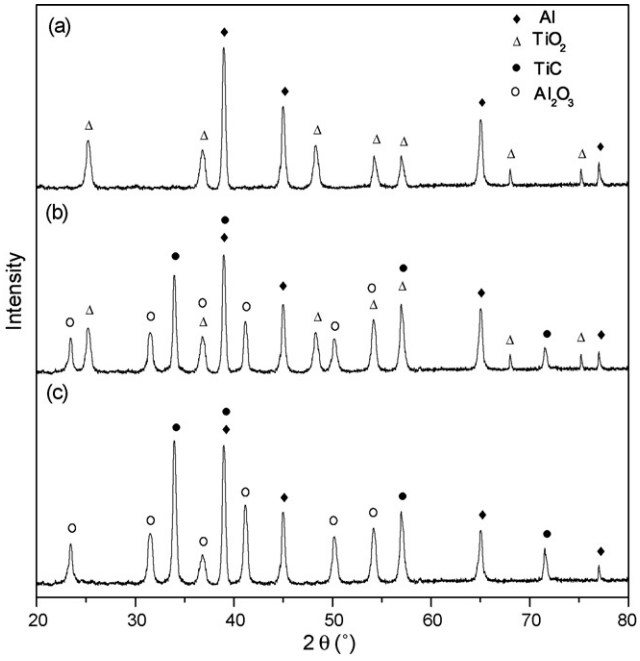

Fig. 5. XRD patterns of different distinct zones quenched: (a) before the combustion front; (b) reaction region; and (c) behind the combustion front.

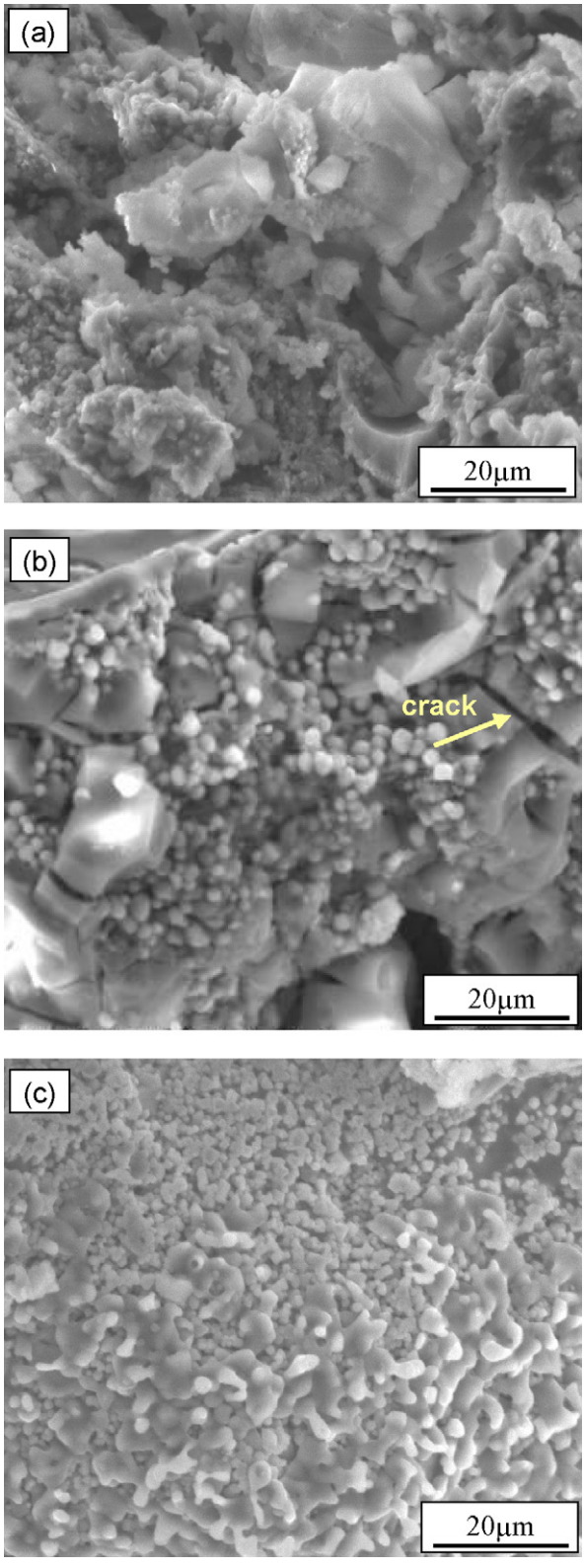

Fig. 6. Microstructure photographs of different distinct zones quenched: (a) before the combustion front; (b) reaction region; and (c) behind the combustion front.

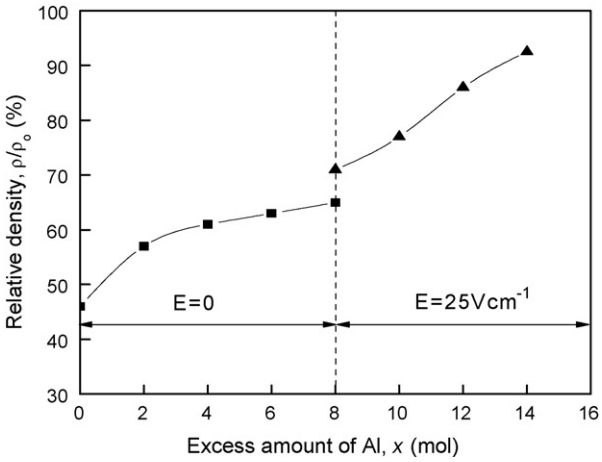

Fig. 7. The dependence of the synthesized composites relative density on excess Al content and field strength.

of a field extended the upper limit of x. This testifies the electric field can overcome the thermodynamic limitation of SHS and make the reaction with $x > 10$ mol possible, which cannot be self-sustained otherwise.

DTA curve of TiO_2–C–Al reactive system is shown in Fig. 2. The endothermal peak at about 660 °C is corresponding to melting point of Al. With the increasing temperature, the reaction between the molten Al and TiO_2 occurs:

$$Al_{(l)} + TiO_2 \rightarrow Al_2O_3 + [Ti]$$

According to Ti–Al equilibrium phase diagram, the displaced [Ti] may react with $Al_{(l)}$ to form interpahses, e.g. $TiAl_3$, TiAl, Ti_3Al. However, as shown in Fig. 3, calculations of the Gibbs energy of Al_2O_3, TiC and $TiAl_3$ show that the binding energy between Ti and C is much stronger than that between Ti and Al at the higher temperature. Hereby, this very likely occurs by the following reactions:

$$TiAl_{3(s)} + C_{(s)} \rightarrow TiC_{(s)} + Al_{(l)}$$

$$[Ti] + C_{(s)} \rightarrow TiC_{(s)}$$

The reactions mentioned above are exothermic, which enhance the formation of TiC without any interphases in the final products. Consequently, the first exothermic peak is corresponding to thermit reaction between Al and TiO_2 and interfacial reaction of Al and [Ti], whereas, the second exothermic peak corresponding to the formation of TiC.

3.2. Combustion behavior

The experimental results showed that in the case of $x = 14$ mol, at the lower strength field less than 12 V cm^{-1}, no SHS reaction takes place, but at and above this threshold, combustion occurs in different modes. When the field strength is in the range from 12 to 31 V cm^{-1}, the combustion reaction carries out in a self-sustaining mode. The rate of self-sustaining reaction makes approximately a linear increase with the increasing field strength, as shown in Fig. 4. When the field strength is up to 31 V cm^{-1}, or higher, no ignition source is required any more. This means that Joule heating of the field itself can initiate the reaction and the so-called thermal explosion or simultaneous combustion takes place.

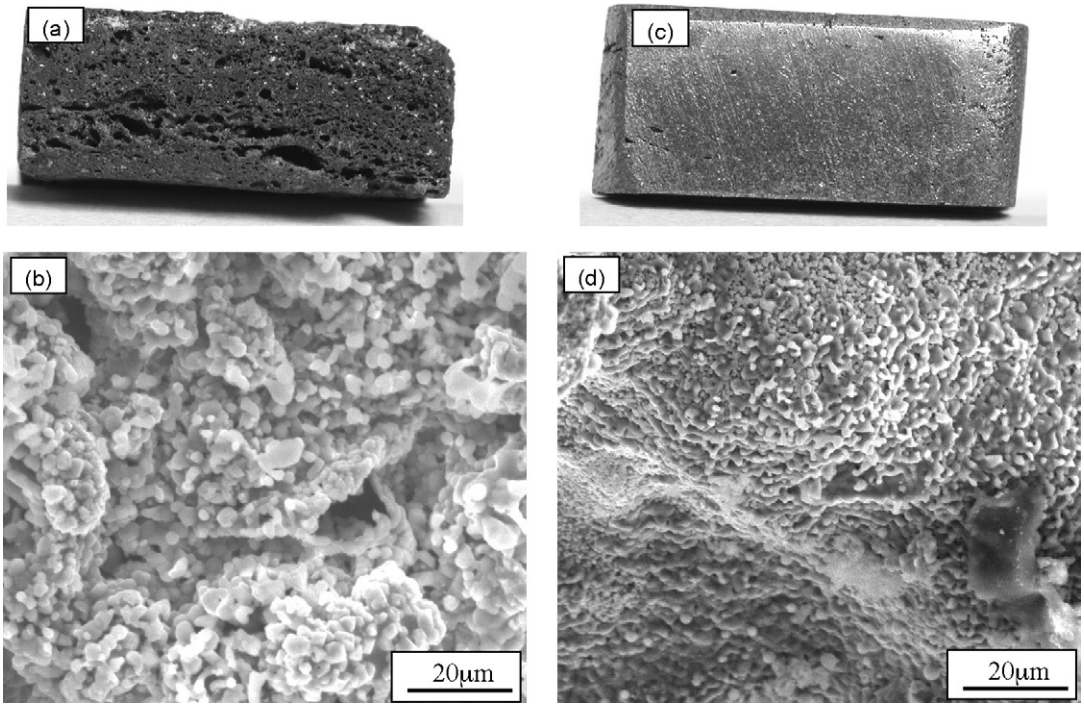

Fig. 8. Macrostructure photographs (a and c) and microstructure photograph (b and d) of the synthesized Al_2O_3–TiC–Al composites under different conditions: (a) and (b) $x = 4$ mol, $E = 0$; (c) and (d) $x = 14$ mol, $E = 25$ V cm^{-1}.

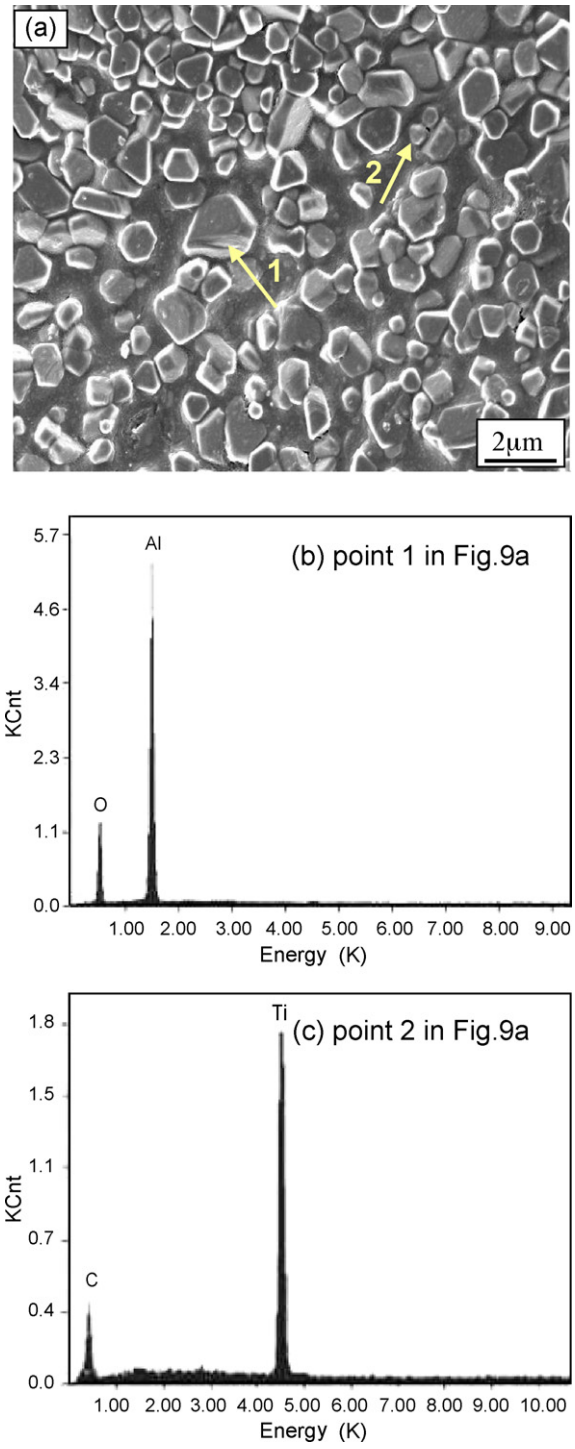

Fig. 9. Microstructure photograph and EDS patterns of the synthesized Al_2O_3–TiC–Al composites with $x = 14$ mol, $E = 25\ V\ cm^{-1}$.

3.3. Microstructures and densification

By means of combustion front quenching method, microstructural evolution of the synthesized TiC–Al_2O_3–Al composite was investigated with a sample under $x = 14$ mol and $E = 25\ V\ cm^{-1}$. Figs. 5 and 6 show the XRD pattern and microstructures within different distinct zones quenched, respectively. Before the combustion front, merely diffraction peaks of TiO_2 and Al (without C) are detected, as shown in Fig. 5a. This means that the reactions did not take place. However, Al had melted and enwrapped other reactants partly. Consequently, as shown in Fig. 6a, after a quick quenching, porosities and even slight cracks form due to shrinkage of liquid Al during solidification. In reaction region, as shown in Fig. 5b, the diffraction peaks of TiC and Al_2O_3 are observed. Whilst, remaining of TiO_2 and Al indicates that the reactions were intermitted owing to quenching. Fig. 6b shows that the reaction region is characterized by formation of fine TiC and Al_2O_3 particles bound by molten Al. Behind the combustion front, the reactions are complete and the diffraction peaks comprise of TiC, Al_2O_3 and Al (Fig. 5c). Due to infiltration of liquid Al into porous TiC–Al_2O_3 product, a dense composite was obtained (Fig. 6c). In general, the formation of Al_2O_3–TiC–Al composite could be staged as: Al is molten first, and reacted with TiO_2 to form Al_2O_3, followed by the formation of TiC through the reaction between the displaced Ti and C.

Fig. 7 shows the effect of excess amount of Al and electric field strength on the relative density of the FACS-ed TiC–Al_2O_3–Al composite. The diagram is classified into two regions, with or without the application of field. In absence of a field, the relative density of the composite slightly increased from 53% to 69% when the excess Al content varied from 2 to 8 mol. Moreover, greater enhancement of densification was achieved with field strength of $25\ V\ cm^{-1}$, during which the relative density increased almost linearly from 72% to 92.5% when the excess Al content increased from 8 to 14 mol. The macrostructure and microstructure of the synthesized TiC–Al_2O_3–Al composites under different conditions are shown in Fig. 8. When $x = 4$ mol and no field was applied, the synthesized composite is porous (Fig. 8a and b) and the relative density is only 59%. On the one hand, the molten Al could bond the TiC and Al_2O_3 particles together to favor the densification. On the other hand, relatively less content of excess Al (e.g. $x = 4$ mol) was not enough to fill completely in the pores produced during the SHS process. Simultaneously, under conditions of $x = 14$ mol and $E = 25\ V\ cm^{-1}$, the synthesized composite is

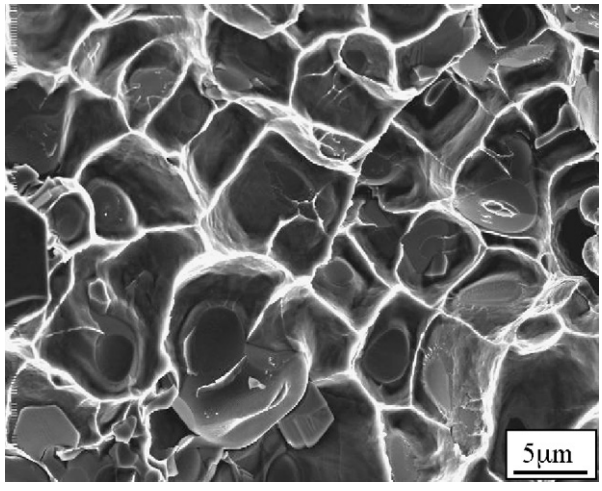

Fig. 10. SEM photograph of fracture surface of the synthesized Al_2O_3–TiC–Al composite.

Table 1
Room-temperature mechanical properties of the synthesized Al_2O_3–TiC–Al composite

	Grain size (μm)	Relative density (%)	Hardness (GPa)	Bending strength (MPa)	Fracture toughness (MPa $m^{1/2}$)
$x=0$, $E=0$	–	46	–	–	–
$x=14$ mol, $E=25$ V cm^{-1}	0.2–1.0	92.5	56.5	531	10.96

dense (Fig. 8c and d) and the relative density is up to 92.5%. It is believed that this is owing to enough molten Al infiltrating into the product and the Joule heating provided by the field. The presence of molten Al strengthens the interconnections between particles and prompts diffusions of reactants. It is electric field with Joule heating that enhances mass transportation between solid and liquid through electromigration, and markedly affects the process of reaction and the microstructure of the products. Fig. 8 shows that the grain sizes of the TiC and Al_2O_3 particles decrease significantly with the increasing field strength. It is believed that the decrease in particle size is the result of higher cooling rates due to the reactive time shortening, associated with the higher velocity of the self-propagating wave with the increasing field strength, which results in the increase of practical combustion temperature as well. The microstructure and EDS pattern of the polished sample with $x=14$ mol and $E=25$ V cm^{-1} are shown in Fig. 9. Semi-quantitative analysis shows that the larger and irregular particle (Point 1 in Fig. 9a) consists of Al and O (Al/O atomic ratio about 1:1.491), whereas the smaller and spherical one (Point 2 in Fig. 9a) consists of Ti and C (Ti/C atomic ratio about 1:1.058). Therefore, it is deduced that the larger particle and the smaller one are Al_2O_3 and TiC, respectively. This means that the reaction is complete and the anticipant composite has been directly fabricated, which is evidenced in the corresponding XRD analysis results, as shown in Fig. 5c. From Figs. 8 and 9, it can be estimated that the real total volume contents of Al_2O_3 and TiC in the final product with $x=4$ mol are much less than the theoretical ones due to lower relative density. Whereas, they are close to the expectation (around 40%) in the composite with $x=14$ mol. The TiC and Al_2O_3 particles in the synthesized TiC–Al_2O_3–Al composite are fine (0.2–1.0 μm) and distribute uniformly in metal Al, as shown in Fig. 9a.

3.4. Room-temperature mechanical properties

Hardness, bending strength and fracture toughness were tested on polished section of the synthesized TiC–Al_2O_3–Al composite with $x=14$ mol and $E=25$ V cm^{-1}. The bending strength was calculated from the following formula [18]:

$$\sigma_f = \frac{3SP}{2WB^2} \quad (2)$$

where P is the fracture load, W and B are the width and thickness of the specimen and S is the support span in three-point bending. Referring to the standard method for measuring plain-strain fracture toughness of metallic materials, ASTM E-399 [19], the effective fracture toughness was calculated by

$$K_{1C} = \frac{P}{BW^{1/2}} Y\left(\frac{a}{W}\right) \quad (3)$$

where a is the depth of the notch. The meanings of the other parameters are the same as those in Eq. (2). $Y(a/W)$ is the stress intensity coefficient given by the following expression:

$$Y\left(\frac{a}{W}\right) = \frac{S}{W}\left\{\frac{3(a/W)^{1/2}[1.99 - a/W(1-a/W)(2.15-3.93a/W)+2.7(a/W)^2]}{2(1+2a/W)(1-a/W)^{3/2}}\right\} \quad (4)$$

The hardness, calculated bending strength and fracture toughness of the samples are 56.5 GPa, 531 MPa and 10.96 MPa $m^{1/2}$, respectively, as shown in Table 1. Fig. 10 shows the fracture surface of the synthesized sample. It can be observed that the fractograph presents a number of dimples and the fracture mechanism is ductile fracture. It is well known that, during ductile fracture, voids usually nucleate on inclusions, grow and link-up to form the fracture surface. The infiltrated composite had a quite characteristic fracture appearance, in which the aluminum microvoids contain TiC and Al_2O_3 grains. This feature was quite typical of the fracture surface.

4. Conclusions

(1) Combining electric field-activated combustion synthesis with the infiltration of molten Al into the synthesized products, a dense TiC–Al_2O_3–Al composite was prepared directly using TiO_2, C and Al powders as reactants.
(2) For $3TiO_2 + 3C + (4+x)Al$ reaction system, the imposition of an external electric field can improve the adiabatic combustion temperature of the reactive system to induce the SHS reaction and support its self-sustain as $x > 10$ mol in this system.
(3) During the formation of Al_2O_3–TiC–Al composite, Al is molten first, and reacted with TiO_2 to form Al_2O_3, followed by the formation of TiC through the reaction between the displaced Ti and C.
(4) In case of samples with excess Al content $x=14$ mol and field strength $E=25$ V cm^{-1}, highly dense TiC–Al_2O_3–Al composite with relative density of up to 92.5% has been directly fabricated, in which the TiC and Al_2O_3 particles are fine and uniform in metal Al. The hardness, bending strength and fracture toughness of the synthesized TiC–Al_2O_3–Al composite are 56.5 GPa, 531 MPa and 10.96 MPa $m^{1/2}$, respectively.

Acknowledgement

This work was supported by the National Natural Science Foundation of China (No. 50574042).

References

[1] H.J. Feng, J.J. Moore, D.G. Wirth, Metall. Trans. A 23 (1992) 2373–2379.
[2] H.J. Feng, J.J. Moore, Metall. Mater. Trans. B 26 (1995) 265–273.
[3] S.V. Gedevanishvili, Z.A. Munir, Scripta Met. Mater. 31 (1994) 741–743.
[4] H. Xue, Z.A. Munir, Met. Mater. Trans. B 27 (1996) 475–480.
[5] S. Gedevanishvili, Z.A. Munir, Mater. Sci. Eng. A 211 (1996) 1–9.
[6] A.G. Merzhanov, Inter SHS 4 (9) (1995) 323–326.
[7] Y. Choi, J.K. Lee, M.E. Mullins, J. Mater. Sci. 32 (1997) 1717–1724.
[8] Z.Y. Fu, H. Wang, W.M. Wang, Acta Mater. Compos. Sin. 14 (1997) 61–64.
[9] E.A. Olevsky, E.R. Strutt, M.A. Meyers, J. Mater. Process. Technol. 121 (2002) 157–166.
[10] D. Horvitz, I. Gotman, E.Y. Gutmanas, N. Claussen, J. Eur. Ceram. Soc. 22 (2002) 947–954.
[11] Z.A. Munir, U. Anselmi-Tamburini, Mater. Sci. Rep. 1 (1989) 277–365.
[12] Z.A. Munir, Mater. Sci. Eng. A 287 (2) (2000) 125–137.
[13] S.V. Gedevanishvili, Z.A. Munir, Mater. Sci. Eng. A 242 (1998) 1–6.
[14] I.J. Shon, Z.A. Munir, Mater. Sci. Eng. A 202 (1995) 256–261.
[15] S.V. Gedevanishvili, Z.A. Munir, Mater. Sci. Eng. A 246 (1998) 81–85.
[16] R. Orru, G. Cao, Z.A. Munir, Chem. Eng. Sci. 54 (15–16) (1999) 3349–3355.
[17] Q. Hu, P. Luo, Y. Yan, J. Alloy Compd. 439 (2007) 132–136.
[18] R. Fu, T.Y. Zhang, Acta Mater. 48 (2000) 1739–1740.
[19] ASTM E-399-83, Annual Book of ASTM Standards, Section 3. American Society for Testing and Materials, Philadelphia, PA, 1984.